Monitoring crustal CO_2 flow: methods and their applications to the mofettes in West Bohemia

Tomáš Fischer, Josef Vlček, Martin Lanzendörfer

Charles University, Faculty of Science, Prague, Czechia

Abstract Monitoring of CO_2 degassing in seismoactive areas allows the study of correlations of gas release and seismic activity. Reliable continuous monitoring of the gas flow rate in rough field conditions requires robust methods capable of measuring gas flow at different types of gas outlets such as wet mofettes, mineral springs and boreholes. In this paper we focus on the methods and results of the long-term monitoring of CO_2 degassing in the West Bohemia/Vogtland region in Central Europe, which is typified by the occurrence of earthquake swarms and discharge of carbon dioxide of magmatic origin. Besides direct flow measurement using flowmeters, we introduce a novel indirect technique based on quantifying the gas bubble contents in a water column, which is capable of functioning in severe environmental conditions. The method calculates the mean bubble fraction in a water-gas mixture from the pressure difference along a fixed depth interval in a water column. Laboratory tests indicate the nonlinear dependence of the bubble fraction on the flow rate, which is confirmed by empirical models found in the chemical and nuclear engineering literature. Application of the method in a pilot borehole shows a high correlation between the bubble fraction and measured gas flow rate. This was specifically the case of two coseismic anomalies in 2008 and 2014, when the flow rate rose during a seismic swarm to a multitude of the pre-seismic level for several months and was followed by a long-term flow rate decline. However, three more seismic swarms occurring in the same fault zone were not associated with any significant CO_2 flow anomaly. We surmise that this could be related to the slightly farther distance of the hypocenters of these swarms than the two ones which caused the coseismic CO_2 flow rise. Further long-term CO_2-flow monitoring is required to verify the mutual influence of CO_2 degassing and seismic activity in the area.

1. Introduction

Long-term monitoring of crustal fluids activity provides a unique opportunity to better understand the relationships among tectonic processes, seismic activity and migration of fluids in the Earth crust. Carbon-dioxide of deep origin represents a link between deep seated magmatic sources of CO_2, the fluid migration paths in the crust, which are controlled by the tectonic stress field, and the earth surface. The presented study is focused to monitoring of CO_2 degassing in the West Bohemia/Vogltand area, which is located in the western part of the Bohemian Massif (BM), the largest coherent surface exposure of basement rocks in central Europe. The western BM is hosting a junction of three tectonometamorphic units, Saxothuringian, Teplá-Barrandian and Moldanubian (Franke, 2000). It is intersected by two regional tectonic structures, the NE-SW trending Eger Rift (ER) and NNW-SSE trending Mariánské Lázně Fault (MLF) (Fig. 1).

The Tertiary ER is a 300 km long striking structure characterized by elevated heat flow and Cenozoic volcanism and its formation is thought to be related to Alpine collision (Ziegler, 1992). The Late-Variscan MLF was reactivated several times during the geological history up to Cenozoic when it participated in the formation of the Cheb Basin (CB). CB is typified by a blocky structural fabric due to a network of faults. Besides the NNW and NW morphologically expressed marginal faults also faults striking NE, E-W and N-S were identified within the basin (Špičáková et al., 2000; Bankwitz et al., 2003).

The present geodynamic activity is manifested by earthquake swarms, massive CO_2 degassing of mantle origin and Quaternary volcanism (Fischer et al., 2014). Seismic activity in the form of earthquake swarms is concentrated in the area of CB, in particular the Nový Kostel focal zone (Fig. 1), where more than 80% of seismic energy is released in frames of the whole seismogenic region. Here the hypocenters form a N-S trending, steeply dipping belt in the depth range from 6 to 10 km; however, no clear fault outcrop has been identified that would match the focal zone geometry. The prevailing focal mechanisms coincide very well with the orientation of the fault zone striking 169° derived from the hypocenter trend. Inversion of focal mechanisms for stress field yields maximum compression direction in the range N135–155°E, which coincides well with the average direction N144°E in Western Europe (Fischer et al., 2014). This direction is however parallel to the strike of the MLF, which indicates a passive role of the MLF in the present stress field (Vavryčuk, 2011).

The strongest earthquakes usually do not exceed M_L 4.5, as was the case of all the eight major instrumentally recorded swarms between 1985 and 2018.

The concentration of the geodynamic phenomena in this small region is not clearly understood. Some authors relate this seismic activity to intersecting crustal faults (e.g., Bankwitz et al., 2003) or to fluids of mantle origin (e.g., Bräuer et al., 2003; Babuška et al., 2016), which could originate from active magmatic underplating (Hrubcová et al., 2017). The degassing occurs in the form of CO_2-rich mineral waters and wet and dry mofettes in several degassing fields. Carbon dioxide is the carrier phase for mantle-derived minor components such as helium, the isotope ratios of which are the best tool to determine whether the fluids are of crustal or mantle-derived origin; high $^3He/^4He$ ratios indicate that ascending gases are of mantle origin (Bräuer *et al.*, 2003). The highest portions of mantle-derived helium (up to 6 R_a, where R_a corresponds to the $^3He/^4He$ ratio of the atmosphere) were found in the CB; the KV degassing center has the lowest $^3He/^4He$ ratios of 2.5 R_a. Lower He-isotope ratios (e.g. $^3He/^4He$ < 6Ra) probably reflect the gas mixing

66 with crustal-derived He along fluid pathways (Bräuer *et al*., 2008). Also, the $\delta^{13}C$ values in the CO_2-rich gas escapes

67 indicate their origin in the upper mantle (Weinlich *et al.*, 1999; Bräuer *et al.*, 2003). CO_2 flow monitoring in West

68 Bohemia has been conducted since the 1990s in a rather discontinuous way. The longest-running observation project

69 is probably the monitoring of Radon activity in Bad Brambach (Heinicke and Koch, 2000; Koch et al., 2003), which

70 has been conducted since 1989.

71 Gas flow is concentrated in three degassing centers: Cheb Basin, Mariánské Lázně, and Karlovy Vary (KV) (Weinlich

72 *et al.*, 1999; Geissler *et al.*, 2005; Kämpf *et al.*, 2007). They are characterized by a high gas flow with daily discharge

73 of dozens of tons of gas (Nickschick et al., 2015) with CO_2 concentrations of more than 99 vol. %. Cheb Basin also

74 has the highest concentration of seismic activity, which makes it ideal for studying the relations between seismicity

75 and gas flow. Interestingly, many studies of the local earthquake swarms show that they may be related to pressurized

76 fluids in the crust and the ascent of gas. This has been pointed out by numerous researchers including Špičák and

77 Horálek (2000), Hainzl and Fischer (2002), Fischer and Horálek (2005) and Hainzl et al. (2016), based on space-time

78 analysis of the seismicity, Horálek et al. (2002), Vavryčuk (2002) and Vavryčuk and Hrubcová (2017), on the basis

79 of moment tensor analysis, and Dahm and Fischer (2014), and Bachura and Fischer (2016), based on Vp/Vs analysis

80 of the volume of hypocenters. The last two studies show that compressible fluids are required to explain the low

81 velocity ratio observed in the course of seismic activity.

82 Another long-time monitoring was carried out as part of the "Research of CO_2 pressure field in the area of West

83 Bohemian spas" project funded by the Ministry of the Environment of the Czech Republic from 1996 to 2005. Gas

84 flow in open boreholes and gas pressure in closed boreholes was monitored at 11 gas escape sites in the Cheb Basin

85 and near Mariánské Lázně (Škuthan et al., 2001, Hron et al., 2006). Monitoring of pressure in a closed well was

86 preferred at many project sites since the functioning of mechanical flowmeters was unreliable due to condensation

87 and freezing. A different type of CO_2 flow monitoring was carried out by Faber et al. (2009), who measured diffuse

88 gas flow by determining CO_2 concentration in soil gas at two stations in the Nový Kostel fault zone. CO_2 flow

89 monitoring was also conducted by Heinicke (personal communication) in the Bublák mofette from 2008 to 2014 by

90 recording the acoustic noise of bubbles below the water table, a method which is similar to that used by Koch et al.

91 (2003). No convincing observation of seismogenic CO_2 flow anomaly was, however, presented in the above-

92 mentioned studies.

93 Mapping of CO_2 emanations was conducted in the area by Nickschick et al. (2015). They used an infrared gas analyzer

94 and accumulation chambers to measure CO_2 flux and CO_2 soil concentration in the mofette field of Hartoušov and

95 found that the diffuse gas flow in dry vents accounts for a high portion of the mofette field's total gas production.

96 The measurement of CO_2 flow presented in this paper began in 2009 in the Hartoušov mofette field with the use of a

97 laboratory chamber flowmeter. Despite problems from the condensation of moisture and freezing temperatures, which

98 resulted in time series gaps, we observed a massive post-seismic CO_2 flow increase shortly after the first M_L 3.5

99 mainshock of the 2014 seismic sequence. A comparison with the fault valve model showed a striking fit, which

100 indicated that the earthquake fracture released gas accumulated in the reservoir beneath hypocenters (Fischer et al.,

101 2017). This gave us a reason to extend the monitoring and test different, more durable, gas flow measurement methods.

102 In this paper, we introduce the principles for our approaches and give a basic comparison of them. We also present

103   the data recorded from the Hartoušov, Bublák, Soos and Prameny stations (see Fig. 1) and evaluate their response to
104   air pressure and temperature and their possible relation to seismicity.
105

2. Data and methods

106

107   Two types of CO_2 degassing are observed in West Bohemia/Vogtland: (i) diffuse gas flow in soil and (ii) massive gas
108   discharge in mofettes and mineral springs. While gas diffusion in soil is influenced by soil moisture and other local
109   conditions, among other factors, gas flow in massive sources is independent of environmental conditions and should
110   reflect the influence of the gas source at in the depth. The deep roots of CO_2 mofettes were also documented by a
111   massive increase in CO_2 flow in the Hartoušov mofette that began about four days after the start of seismic activity in
112   2008 and 2014 (Fischer et al., 2017). This points to the relatively fast speed of gas migration in the upper crust and
113   qualifies mofettes as favorable places to monitor the amount of leaking gas. Since 2015, the current monitoring at
114   Hartoušov has been extended to other places in order to provide robust measurements capable of recording possible
115   future gas anomalies at multiple sites. Because the conditions differed among the monitored sites, different
116   measurement methods were designed. In this study, we distinguish between *direct* and *indirect* gas flow measurement
117   methods (Camarda et al. 2006). The direct methods directly record the volume of gas per minute and require that gas
118   flow be captured by a funnel or borehole. The indirect methods either involve deriving gas flow from the bubble
119   fraction in water (pressure probes are placed beneath the water table), or rely on measuring gas overpressure in a
120   closed borehole or, finally, they calculate CO_2 flux from the concentration of gradients in the soil (Baubron et al.,
121   1990). The dynamic concentration method is based on measuring the CO_2 content in a mixture of soil gas and air
122   obtained by a special probe placed vertically in the soil. The dynamic concentration is proportional to the soil CO_2
123   flux according to an empirical relationship, which depends on soil permeability (Gurrieri and Valenza, 1988).
124
125   *Figure 1 .*

2.1 Monitoring network

126

127   Five gas escape sites were monitored in the period described: *Hartoušov, Bublák, Soos, Dolní Částkov* and *Prameny*
128   (see the map in Fig. 1 and photos in Fig. 2). While the first three are located in mofette fields, the remaining are
129   boreholes which tap mineral spring sources.
130   The pilot site of *Hartoušov* is located in a wooden hut above a 28.2 m deep F1 borehole, which taps a CO_2 saturated,
131   pressurized aquifer. The plastic borehole casing, with an inner diameter of 115 mm, is perforated in the depth range
132   of 20-28 m. Water level measurements date back to 2007, and gas flow has been measured here using a drum chamber
133   gas flowmeter since 2009. The sensitivity of this type of instrument to environmental conditions (freezing or
134   evaporation of the working liquid) caused gaps in the recorded time series. Since 2013, there have only been brief
135   gaps thanks to the use of a different type of working liquid, improvements in the condenser separation and thermal
136   insulation. This direct field gas flow measurement is used as a reference for testing different flow measurement devices
137   prior to their installation at other sites. Additional permanent measurements include water pressure in several depth

levels, water temperature and air temperature and pressure. In 2016, a 108.5 m deep borehole F2 was drilled in the Hartoušov mofette with the aim of studying geo-bio interactions (Bussert et al., 2017). It showed a CO_2 overpressure of 5 bars and was converted to a closed monitoring borehole with continuous measurements of downhole pressure and temperature and wellhead pressure. A broadband seismometer was installed in 70 m depth in the year 2019.

The *Bublák* station has been located in a natural mofette in a swamp since 2015. To avoid interfering with natural conditions at this site, the equipment is buried underground, which does not allow for direct gas flow measurement. Instead, the differential water level is measured and used as a proxy for the volumetric fraction of free gas in water, see section 2.3. Because of the rising bubbles, the water does not freeze in winter, making this measurement quite stable. The *Soos* station has been located in a natural mofette field since 2015, and the gas from a single mofette is captured by a funnel allowing for direct gas flow measurement. The small size of the metal box shelter and the need to use battery power, however, do not make it possible to prevent the freezing of the system in winter. The water level and temperature in the mofette and the volumetric fraction of free gas are measured here using an electric resistivity probe. In *Dolní Částkov*, the gas escapes both through a shallow borehole and the surrounding soil, which makes the flow measurements rather unstable. The *Prameny* station is located on top of a 100 m deep closed borehole (HJ-3A, drilled 1994) with degassing mineral water. Conditions at this site allow only for the measurement of the water level, temperature and wellhead gas pressure, which have been available since 2009.

Figure 2 .

Table 1. CarbonNet monitoring network.

Station name and code	Environment	Methods
Bublák *BUB*	*Natural mofette*	*Water temperature, two pressure heads (sensor depths 0.7 and 1.4 m)*
Hartoušov *HAR*	*30m deep open borehole VP8303 (F1)*	*Air temperature, barometric pressure, three pressure heads (sensor depths 4.45, 5.45 and 27.2 m), water temperature, gas flow rate, differential pressure in the well*
	108.5m deep closed borehole HJB-1 (F2)	*Pressure head (sensor depth 92m), water temperature, absolute wellhead pressure, seismometer*

Prameny PRA	100m deep open borehole HJ-3A	Pressure head (sensor depth 4.5 m), water temperature, absolute wellhead pressure
Soos SOO	Natural mofette	Pressure head (sensor depth 1.5 m), water temperature, water resistivity
Dolní Částkov DCA	10 m deep open borehole	Gas flow rate

157

2.2 Direct CO$_2$ flow measurement methods

159 Long-term gas flow monitoring in the field must meet various requirements. It should provide sufficiently accurate
160 data of gas flow, which may contain dirt particles and moisture in changing field conditions of temperature, humidity
161 and air pressure. The presence of carbon dioxide further creates a highly corrosive environment, which the sensors
162 should withstand. Commercial flowmeters are usually not designed to meet these demands. We have tested (at SOOS
163 and Dolní Částkov stations) the *MEMS* (Micro-Electro-Mechanical Systems) *flowmeter*, which is based on heat
164 convection in moving gas. It works on the principle of a wheatstone bridge, where changes in the resistivity of the
165 resistor are measured according to the temperature changes caused by the flow of gas through a heater placed in the
166 middle of the sensor (Dmytriw et al., 2007). These low-cost sensors, however, failed in our tests. None of the MEMS
167 flowmeters tested measured for longer than 4 months, despite the installation of filters to capture solid particles and
168 moisture from the gas before entering the sensor. A popular way of measuring gas flow is the *Venturi type flowmeter,*
169 which works by measuring the drop-in pressure at a constriction in a tube. Our tests of similar devices failed due to
170 temperature drifts of the sensor and electronics, which were of the same order as the CO$_2$ flow variations. Direct flow
171 measurement methods also include the *acoustic method* based on the Doppler effect, which is commonly used for
172 water flow measurement. This, however, does not appear to be suitable for gas, which contains fewer particles acting
173 as diffractors than liquid.
174 The standard *flowmeters with rotating mechanical parts* driven directly by the gas flow were also found not suitable
175 due to the corrosive CO$_2$ environment. Better performance was achieved with a *drum-type chamber flowmeter*, which
176 contains a revolving measuring drum within a packing liquid (we use low-viscosity oil). The measuring drum
177 compulsorily measures volume by periodically filling and emptying four rigid measuring chambers. This *chamber*
178 *laboratory instrument* was found suitable for field measurement, where sufficient space and non-freezing temperatures
179 can be guaranteed. It has been used as the primary flowmeter at the Hartoušov F1 borehole   .

180

181 **2.3 Indirect CO_2 flow measurement methods**

182 **Gas pressure in a closed borehole**

183 In a closed borehole tapping a gas-saturated aquifer an overpressure builds up whose magnitude has been speculated

184 to reflect the amount of gas entering the aquifer from below (e.g. Hron and Škuthan, 2006). However, a profound

185 discussion of how exactly the deep CO_2 leakage affects the measured overpressure is still absent, to the best of our

186 knowledge. Considering a CO_2 flux $q = q_1 + q_2$ summing the flux through the top of the aquifer in the vicinity of the

187 borehole, q_1 and the possible gas leakage through the borehole, q_2, and assuming simply that the borehole overpressure

188 p is proportional to the both, then p follows the equation

189
$$p = \frac{q}{K_1+K_2},$$

190 where K_1 and K_2 are the permeability factors related to the ceiling of the aquifer and to the borehole sealing,

191 respectively. Hence the measured overpressure is proportional to the gas flux controlled by deep processes, but also

192 influenced by the permeability of the superficial layer as well as by any possible leaks through the wellhead. In

193 particular, any variation in sealing layer properties, caused e.g. by the actual weather conditions, is then directly

194 projected onto the pressure measured.

195 Accordingly, in spite of the easy implementation of the pressure measurements in a closed borehole, we used this

196 method only at the *Prameny* site, where technical and logistic conditions did not allow the installation and maintenance

197 of a flow measurement. Excessive influence of K_1 on the measured pressure can be suppressed by introducing a

198 controlled leakage in the wellhead, which ensures that K_2 is not small in comparison to K_1 as has been implemented

199 at *Prameny* station.

200

201 **Bubble fraction in water**

202 We have used the bubble fraction monitoring method since observing a striking coincidence between the gas flow rate

203 and groundwater level (see later in this paragraph) increase in the Hartoušov F1 borehole during the 2014 seismic

204 sequence (Fischer et al., 2017). Within a few months after the beginning of the sequence, the gas flow rate in the

205 borehole increased fivefold and the measured water level by more than 1 m. Since then, both quantities have indicated

206 an overall gradual decrease back to their original levels.

207 Instead of the notion of groundwater level, adopted in Fischer et al. (2017) and other works, we stick to the more

208 strictly defined terms *pressure head* and *hydraulic head* in the present paper, which is due a few explanatory

209 comments. Within a steady water column resting in a borehole (or a narrow mofette), the hydraulic head (defined as

210 the sum of the pressure head and elevation) is independent of the elevation and is referred to as the groundwater level,

211 as it coincides with the elevation of the free water surface observed in the borehole. This is why the exact elevation of

212 the actual placement of the pressure probes in the borehole is usually disregarded, and the term groundwater level is

213 used somewhat loosely without risk of any confusion. In the case of a continuous bubbly flow through the borehole,

214 however, hydraulic head is not a depth-independent quantity, but rather inevitably increases with elevation. An

215 intuitive explanation is that the mean density of the water - gas bubbles mixture is markedly lower than that of water

216   (this is, however, merely an approximation, see also section 2.5). Following this simple concept, the density of the
217   mixture would be (disregarding the density of the gas CO_2 as negligible)

218
$$\varrho(z) = (1 - \phi(z))\varrho_w, \tag{1}$$

219   where $\phi(z)$ denotes the volumetric fraction of bubbles in the water column profile at elevation z, and ρ_w stands for
220   the mass density of the water in the well (say, clear water at a given constant temperature). Denoting by $\psi(z)$ the
221   pressure head, related to the actual pressure $p(z)$ through $p(z) = \rho_w g \psi(z) + b$ with g being the gravitational
222   acceleration and b the barometric pressure (Fig. 3a), and denoting by $h(z) = \psi(z) + z$ the hydraulic head, we assert
223   that the difference in the measured pressures, pressure head and hydraulic head equals

224
$$p(z_1) - p(z_2) = p_1 - p_2 = \int_{z_1}^{z_2} \rho(z)\, g\, dz$$

225
$$\Rightarrow \quad \psi_1 - \psi_2 = \int_{z_1}^{z_2} (1 - \phi(z))\, dz \tag{2}$$

226
$$\Rightarrow \quad h_2 - h_1 = \int_{z_1}^{z_2} \phi(z)\, dz,$$

227   i.e. the hydraulic head $h(z)$ measured in the borehole increases with elevation by a factor equal to the volumetric
228   fraction of the bubbles in the borehole profile. Here, for the sake of brevity, we abstract from the time dependence of
229   all quantities.

230   *Figure 3*

231

232   The mean bubble fraction within the measured section of the water column can thus be defined as

233
$$\phi_{12} = \frac{h_2 - h_1}{z_2 - z_1} = 1 - \frac{\psi_1 - \psi_2}{z_2 - z_1} \tag{3}$$

234   As the ascending gas bubbles expand due to the decreasing pressure, both the volumetric flux of the gas and the bubble
235   fraction $\phi(z)$ increase correspondingly with elevation. In order to obtain a quantity independent of the depths of the
236   pressure probes, a further correction needs to be applied. A reasonable approximation can be obtained based on the
237   following simplification. We assume that the gas expands isothermally, so that its volumetric flux is inversely
238   proportional to pressure, and that the bubble fraction is approximately proportional to the volumetric flux, so that we
239   can write

240
$$\phi(z) = \phi_0 \frac{p_0}{p(z)}$$

241   where Φ_0 represents the bubble fraction at the reference pressure p_0 (which we later set as 100 kPa). Further,
242   approximating the pressure profile between the two pressure probes by a linear function

243

244
$$p(z) = p_1 + \frac{z - z_1}{z_2 - z_1}(p_2 - p_1)$$

245

246   we obtain (by substituting $\phi(z)$ to (2) and integrating) the formula for Φ_0, let us call this the projected bubble fraction,

247

248
$$\phi_0 = \phi_{12} \frac{p_2 - p_1}{p_0 \ln\ln\left(\frac{p_2}{p_1}\right)} \tag{4}$$

249

250 One should note that the quantity obtained here is subject to some uncertainty due to a number of simplifications, and

251 that it only gives the approximated volumetric fraction and not the gas flow rate itself (see section 2.5).

252 In the Hartoušov F1 borehole, the pressure head had been measured until September 2018 by one pressure gauge in

253 the depth of 8 meters, well above the bubble entry point. In Fischer et al. (2017), the corresponding hydraulic head

254 was referred to as the groundwater level. As proposed in the paper, we split its time variation into two parts: the

255 variation (a) of the hydraulic head $h_e(t)$ at the bottom of the bubble flow column and (b) of its increase through the

256 column due to the gas bubbles. The optimal solution to obtain data for (a), which was implemented in Hartoušov F1

257 in late 2018, is to measure the pressure head in a depth beneath the bubble entry point directly by a dedicated pressure

258 probe (Fig 3b). While direct measurement was unavailable, it was supposed that (a) is given only by the surrounding

259 hydrogeologic situation and is unaffected by the gas flow. A single measurement of the pressure at the bubble

260 occurrence depth by Fischer et al. (2017), corrected by a continuous pressure head record from a nearby observation

261 well in Hrzín 8 km apart, which is not affected by the CO_2 gas flow, was used as $h_e(t)$. Note that $h_e(t)$ also describes

262 the hydraulic head in any depth beneath the occurrence of bubbles. While Fischer et al. (2017) considered the

263 possibility that the gas exsolution depth varies with time, we argue here (see section 2.4) that the gas bubbles have to

264 appear at the penetrated section of the Hartoušov F1 borehole. This allows us to determine the mean volumetric

265 fraction of the bubbles using eq. (3) with $h_1(t) = h_m(t)$ being the hydraulic head measured at the depth $d_m = 4$ m, and

266 $h_2(t) = h_e(t)$ being the hydraulic head measured at the bubble entry depth (or anywhere below), which we suppose to

267 be at the upper part of the penetrated section at $d_e = 20.5$ m (Fig.3).

268 In Fig. 4 the record of $h_e(t)$ and $h_m(t)$ and the resulting projected bubble fraction $\phi_0(t)$ defined by eq. (4) is shown

269 for the whole period studied in Fischer et al. (2017). We refer to this method as the *integral method.*

270

271 *Figure 4*

272

273 The method presented above is applicable only in boreholes and narrow tube-like mofettes. The borehole should tap

274 the underground water, and there should exist a continuous column of gas bubble flow from certain depth to surface.

275 Also, independent measurement of the hydraulic head in the aquifer/reservoir beneath the bubble flow column should

276 be possible, either in the same well or, at least, in a nearby well free of gas flow. These conditions are not fulfilled in

277 natural mofettes, which are usually only less than 2 m deep and communicate with the surface water significantly. In

278 such cases, the difference of pressure heads along a fixed depth interval *within* the bubble flow column can be

279 measured and used to define the mean bubble fraction $\underline{\phi_{12}}(t)$ and the projected bubble fraction $\phi_0(t)$.

280 This *differential method* has been tested in the Hartoušov F1 well and Bublák mofette stations since 2015 using two

281 analog water-level sensors attached at a 1-meter distance on a metal rod. The obvious disadvantage is that both

282 measurements (instead of just one) are subject to fluctuation due to the bubbly flow, and that the noise in the resulting

283 bubble fraction data is inversely proportional to the distance between the probes. To suppress the noise, an RC circuit

284 with a 100 s time constant is applied.

285 An alternative way of determining the bubble fraction is based on the electric resistivity measurement of the water-

286 bubble mixture. Unlike the pressure difference method, this method does not need to be focused on the vertical chain

of bubbles, but it can assess the fraction of bubbles in a 3D volume defined by the geometry of electrodes. For this purpose, two water resistivities are measured by a special probe in the mofette: the reference resistivity of the water free of bubbles R_R and the resistivity of the water-bubble mixture R_M. The bubble fraction is then derived as

$$\phi(t) = 1 - c\,\frac{R_R(t)}{R_M(t)}$$

where c is the geometric calibration constant. This type of measurement has been tested in the Soos mofette since 2015.

2.4 Depth of gas bubbles appearance

It is possible to speculate that the exsolution of the gas bubbles from the water with dissolved CO_2 takes place at a certain depth in the borehole, while below that depth the pressure is sufficient to contain the CO_2 in the dissolved phase. In this view, the exsolution depth d_e could vary in time, as considered by Fischer et al. (2017), following variations of $h_e(t)$ and of the CO_2 supply from the reservoir. Let us note, however, that such a scenario is only possible for gas fluxes much lower than those observed in the Hartoušov F1 borehole.

Assuming a steady flow of the dissolved CO_2 up through a borehole section with no penetration below d_e, two transport mechanisms can be considered, convection or molecular diffusion. As for convection, no driving force to induce a flow in a water column in a borehole, in particular no significant temperature variations, has been observed in the Hartoušov F1 borehole. The mass flux due to molecular diffusion, on the other hand, can be estimated as follows, and it appears to be very limited. Assuming that the concentration of the dissolved CO_2 in the resting water column increases with increasing depth as much as allowed by the increasing hydrostatic pressure (with the Henry's law constant being of the order of 10^{-5} kg m^{-3} Pa^{-1}, see Sander, 2015), then the corresponding diffusive flow rate (with the diffusivity being of the order of 10^{-9}m^{2}s^{-1}) through the borehole of the given cross-section area (say, 10^{-2} m^2) would be no more than of the order 10^{-12} kg s^{-1}. This is by four orders smaller than the mass flow rate through the borehole section of 1.6 10^{-8} kg s^{-1} estimated on the base of CO_2 flow measurements of Nickschick et al. (2015) who reports the daily flow rate of 50 tons for an area of 350 000 m^2. We thus infer that the gas bubbles enter the Hartoušov F1 borehole in its penetrated section, as we assumed in the previous section or in the presence of significant water discharge, such as in mineral springs.

2.5   T   ests of bubble fraction method

The methodology for indirect gas flow measurement using pressure difference (the differential method) was first tested in the laboratory. The experimental setup consisted of an air pump connected with a valve for controlling the air flow, which was led to the bottom of a plastic tube with an inner diameter of 10.5 cm and a height of 2.5 m simulating the borehole. Two water pressure probes were installed at a fixed distance of 0.5 m on a vertical rod inside the tube and all the air from this tube was led to the chamber gas flowmeter. The air inflow was increased stepwise, and at each level the data were recorded for a period of 15 min using a 1Hz sampling rate. The gas flow ranged from 0 to 30

322   L/min, which corresponds to the volumetric flux ranging from 0 to 0.06 m/s. The observed mean bubble fraction

323   appears to increase nonlinearly with the gas flow (Fig. 5). Note that the modification using (Eq. 4) is insignificant

324   here, due to the fact that both pressure probes are at a depth of less than 1 m. The bubble fraction values are more

325   scattered than the gas flow rate measured by the flowmeter. The resulting noise was partially suppressed by low pass

326   filtering of the pressure data using an RC circuit with a time constant of 30 s and additionally by 1 min data sampling

327   to smooth the water level values.

328   It is worth noting that the dynamics of bubbly flow in a borehole is quite a complex issue, which however appears to

329   have been studied rather intensively in the chemical and nuclear engineering literature (see, e.g., Ghiaasiaan, 2008;

330   Montoya, 2016). The simple considerations introduced in the previous text (Eq. 3 and 4) correspond to the drift-flux

331   model for a vertical borehole, provided that the water flux through the borehole is negligible. In particular, any

332   momentum exchange with the walls is ignored. While this approach is well justified for the bubbly flow regime

333   observed with small gas fluxes, with increasing volumetric gas one observes different flow regimes of greater

334   complexity, such as the slug flow and churn flow. As the bubbles ascend, they increase in volume, join each other

335   merrily or even sadly split apart, their brief life being eventually cut short by obstacles such as the pressure probes

336   dangling in the well; these are however out of the scope of this paper. Even in the bubbly flow regime, the relation

337   between the bubble fraction ϕ and the volumetric flux of the gas bubbles u [m/s] has been described, e.g., by the

338   following well established empirical relation (Zuber and Findlay, 1965).

339    $$\phi = \frac{u}{C_0 u + V_{gj}} \qquad (5)$$

340   where $C_0 = 1.13$ and, assuming that the density of the gas is negligible when compared to that of water,

341    $$V_{gj} = 1.41 \left(\frac{\sigma g}{\rho_w}\right)^{1/4}$$

342   The curve in Fig. 5 is obtained by taking the surface tension for water and air at the laboratory temperature as

343    $\sigma = 0.07$ N/m. It appears that the mean bubble fractions derived from our pressure probe data overestimate the void

344   fractions given by the Zuber-Findlay model, in particular for low flow rates.

345   For comparison, we also show in Fig. 5 the projected bubble fraction data ϕ_0 plotted against the corresponding gas

346   flow rates measured on the Hartoušov F1 borehole. The comparison to the laboratory data and to the Zuber-Findlay

347   model reveals a discrepancy that indicates some need for further analysis, which is beyond the scope of the present

348   study. Let us briefly note that the difference cannot be explained by the mere parametric differences from the

349   laboratory setting such as the temperature, gas and water composition.

350   In Fig. 6 we compare the bubble fractions obtained on the Hartoušov F1 borehole using integral and differential

351   methods. While it appears that the projected bubble fraction data from the Hartoušov F1 site cannot be directly inverted

352   to obtain a reasonable gas flow rate estimate, it is important that they provide a fair correlation (see also Fischer et al.

353   2017 and Fig. 4 in their paper) and can thus provide a valuable gas flow rate proxy. As expected, the integral method

354   data seems to perform better than the differential data (see Section 2.3). Note particularly the high noise of the latter

355   and its lower correlation to the gas flow rate measurement (Fig. 6). Accordingly, using the pressure sensors at a larger

356   distance, and, if possible, placing one of them below the bubble entry depth, seem preferable for indirect gas flow

357   measurement.

358   *Figure 5*

359   *Figure 6*

360

361   **2.6 Environmental effects**

362   The measurements of CO_2 flow, CO_2 pressure and pressure head are influenced by environmental effects – mainly

363   variations of temperature (diurnal, seasonal), changes of barometric pressure and tidal effects. Temperature and

364   barometric changes are the most significant, since their influence can be local and can vary even among the stations

365   of the network. Barometric and tidal loading of aquifers has been studied in detail (e.g. Jacob, 1939; Rojstaczer and

366   Riley, 1990; Roeloffs, 1996). Here, we address the basic principles that are relevant to the pressure and production of

367   the upstreaming gas. Both the confined and unconfined response of pressure head are characterized by the barometric

368   efficiency E_B, which expresses the ratio of the change of the hydraulic head Δh caused by the barometric pressure

369   change Δb

370     $$E_B = \rho_W\, g\, \frac{\Delta h}{\Delta b} \tag{6}$$

371   The net response is always a decrease in the hydraulic head with an increase in barometric pressure. The barometric

372   pressure variations act directly on the open water level in the well and also on the formation composed of the mineral

373   matrix and pore space filled by the water. As a result, the direct effect on the water level in the borehole is partially

374   suppressed by the fraction of the external load borne by the formation water. Hence, the barometric efficiency can

375   also be written as

376     $$E_B = \frac{\theta \beta}{\theta \beta + \alpha} \tag{7}$$

377   where α and β is the compressibility of the rock matrix and water, respectively, and θ represents porosity within the

378   aquifer. Thus, barometric efficiency can be described as the fraction of specific storage derived from the

379   compressibility of water or, equally, as the fraction of external load change borne by the formation either as

380   compaction or expansion. Accounting for the range of fractured rock compressibilities, E_B of confined aquifers usually

381   ranges between 0.2 and 0.7 (Todd, 1980) and may reach 1.0 for granite with a very low compressibility of the rock

382   matrix (Roeloffs, 1996; Acworth and Brain, 2008). Note, however, that large values of E_B may as well correspond to

383   large values of β; this fact is not addressed in the literature for the simple reason that it is usually the rock that varies

384   from site to site and not the water. In this concern, the possible effect of the presence of the compressible CO_2 bubbles

385   within the aquifer surrounding the borehole on the barometric efficiency is a question that has not been addressed in

386   the literature, to the best of our knowledge.

387   Similarly, the barometric effect to the CO_2 discharge from an aquifer through an open well has not been studied either.

388   One can expect that an increase in the pore pressure due to an increase in the barometric pressure allows for larger

389   amounts of CO_2 to be dissolved in water, which in turn decreases the volume of CO_2 leaking into the well. Similarly,

390   a decrease in barometric pressure may induce increased degassing. Note that there exist many unknowns in this regard,

391   such as the flow paths of the gas ascending through the aquifer, the amount of the mobile and immobile gas bubbles

392   in the porous space, etc. In the Hartoušov F1 borehole, a strong anticorrelation between the gas flow rate and the

393   barometric pressure has been observed.

394   We correct the measured quantity f (pressure head or gas flow) for demeaned barometric pressure variations b

395   using the equation $f_c = f - E_B (b - <b>)$. Barometric efficiency E_B is determined with the target of minimum cross

396   correlation of f and f_c. To account for the possible time variation of E_B a sliding window of one day is used; see Fig.

397   7a for original and corrected records of pressure head and gas flow in Hartoušov F1. Fig. 7b shows the cross-

398   correlation functions between barometric pressure and original and corrected records. The success of barometric

399   correction is indicated both by removing the anti-correlation with air pressure and by minimizing short period

400   variations in the corrected records. The mean barometric efficiency was 0.76 for the pressure head and 0.46 L/min/kPa

401   for the gas flow.

402

403   *Figure 7*

404

405   Other external effects like diurnal temperature variations and Earth tides were found much weaker than the influence

406   of barometric pressure. The volumetric fraction of bubbles is not affected by air temperature, since the sensors are

407   placed in groundwater with an almost constant temperature. In addition, the periods of diurnal temperature variations

408   and significant Earth tide components are significantly shorter than the expected durations of anomalies of deep-

409   generated gas flow. Accordingly, we do not apply corrections for temperature variations and Earth tides.

410

411   **3. Results of CO_2 flow monitoring in West Bohemia**

412

413   The time series of gas production at all monitored stations, along with seismicity plot, are shown in Fig. 8. The record

414   at Hartoušov F1 for the period from late 2007 to 2019 shows a long-term decrease interrupted by several abrupt

415   massive increases in gas discharge. The maximum flow, reaching 50 L/min, followed the 2014 seismic sequence in

416   late summer/autumn 2014; the minimum values, below 10 L/min, were observed prior to the 2014 seismic sequence

417   and at the present time. The fast coseismic increase and long-term postseismic decrease are visible both in the gas

418   flow and *integral bubble fraction* data determined using eq. (3) and (4) and are consistent with Sibson's fault valve

419   model (Fischer et al., 2017). Note particularly the abrupt rise in gas flow and CO_2 bubble fraction during the M_L 4.4

420   seismic sequence of May – August 2014 and in bubble fraction during the October 2008 M_L 3.8 swarm. Next to these

421   striking coincidences of seismic activity and CO_2 release we also find cases of strong seismic activity, which was not

422   accompanied by a significant gas flow anomaly (see the M_L 3.4 swarm of 2011 and the most recent M_L 3.8 swarm of

423   2018). On the other hand, the CO_2 flow record shows a few positive pulses which are not related to significant seismic

424   activity (Fig. 8b). The most striking one is the gas production increase in the period from the beginning of May till the

425   end of July 2016, which is visible both in the gas flow and bubble fraction records. This is, however, undoubtedly of

426   anthropogenic origin caused by drilling of the nearby 108.5 m deep F2 borehole at a distance of 40 m from the

427   monitored F1 borehole, which drilling started on March 30 (Bussert et al., 2017). The drilling reached the top of a

428   CO_2 pressured horizon at a depth of 80 m on April 21 and created a shortcut to the shallower aquifer, which was

429   tapped by the monitored borehole. The three-month long gas increase thus represents a delayed response to a nearby

430   drill. Another, less pronounced, positive pulse in the period from mid-September to late November 2016 is of unknown

431   origin. A number of negative pulses and oscillations are found on the bubble fraction record alone, which lower the

432   correspondence between the gas flow rate and the bubble fraction data and indicate a more complex relation between

433   gas flow in a borehole and volume fraction of ascending bubbles, as already noted in section 2.5.

434   The records of gas *differential bubble fraction* data in Bublák and *resistivity-based bubble fraction* in Soos indicate in

435   the monitored period since autumn 2015 a steady gas release with only a few bumps, which are most probably of local

436   origin and related to the shallow character of the mofettes. Gas at these sites passes through approximately cylindrical

437   vents of ~0.5 m diameter and ~1 m depth filled by surface water. The similarity of bubble fraction increase at Soos

438   and gas flow increase at Hartoušov F1 in summer 2016 is most probably merely accidental, considering the

439   anthropogenic origin of the rise at Hartoušov and the large mutual distance of about 5 km of these sites.

440   As mentioned in section 2.3, the integral method of bubble fraction measurement provides better results than the

441   differential method. The latter suffers particularly from high noise caused by the placement of both pressure probes in

442   a water column with flowing bubbles as shown in Fig. 6. One can also notice a better correlation of the integral method

443   compared to the differential one. Unfortunately, due to technical problems, we were not able to perform this

444   comparison for the same time window – so time windows of the same length (3 months) free of any technical issues

445   were selected.

446

447   **4. Discussion**

448   The *barometric efficiency E_B* of the groundwater pressure head of 0.76, which we obtained, is relatively high. The

449   high values of E_B are generally considered an indication of the small compressibility of the rock matrix that is typical

450   for unweathered granite (Acworth and Brain, 2008). The target aquifer is formed by sedimentary formations of the

451   Cheb Basin composed of sandstones and conglomerates with varying clay contents underlain by mica-schist basement

452   (Bussert et al., 2017). The compressibility of these types of rocks is, however, 3 to 6 times greater than of granite

453   (their bulk moduli range from 10 to 20 GPa compared to 50 GPa for granite). Using Eq. (4), porosity 30% and bulk

454   moduli ratio of matrix and pore fluid equal to 5, one gets $E_B = 0.5$. The level $E_B = 0.76$ is reached for bulk moduli

455   ratio of 15. Assuming the bulk modulus of aquifer rocks about 10 GPa, one obtains a bulk modulus of the fluid of only

456   about 0.7 GPa, which corresponds to three times larger compressibility than for water. This could be explained by the

457   presence of carbon dioxide in the groundwaters in gaseous phase and is worth further research.

458   *The gas flow trend* in Hartoušov after the 2014 seismic sequence shows signatures similar to those in the period before

459   2014, which followed the 2008 swarm. A similar, long-term overall decrease is followed by steady state behavior with

460   an almost constant flow rate of about 10 L/min. In terms of the Sibson's fault valve model, this corresponds to the

461   self-sealing phase of the fault due to mineral precipitation (Sibson, 1992) when pressure builds up and in combined

462   action with tectonic loading results in increasing instability of the fault. This inevitably leads to later recurrence of

463   fault failure in the form of seismic activity and regeneration of fault permeability. As indicated above, the coincidence

464   of a massive rise in CO_2 flow and seismic activity has not been observed since the 2014 seismic sequence. Indeed,

465   none of the earthquake swarms since 2014 have been accompanied by a distinct CO_2 degassing anomaly (Fig 8b). All

466   in all, in the whole period of CO_2 flow monitoring in Hartoušov since 2007, five earthquake swarms with magnitude

467   M_L larger than 3.0 occurred (2008, 2011, 2014, 2017, 2018) and only two of them (2008 and 2014) were accompanied

468   by a strong and long-lasting coseismic increase in CO_2 degassing. This is not surprising in general, because the fault

469   valve mechanism might act only under certain circumstances. And even if a fluid pulse is released during every

470   stronger seismic sequence its volume might not be sufficient to reach the Earth's surface with a detectable amplitude.

471   This is also directly related to the pressure buildup in the fluid reservoir beneath the sealed fault, which is a long-

472   lasting process and thus earthquakes that occur soon after releasing the accumulated fluid pressure are likely to not be

473   accompanied by a significant fluid release.

474   In this context it is also of interest to consider the *hypocenter cluster geometry* in 3D and its relation to the presence

475   of permeable channels in a shallow crust allowing crustal fluids to reach the surface. In Fig. 9 hypocenters of individual

476   earthquake sequences are indicated in a vertically oriented cross section and show a hat-like structure in depths from

477   6.0 to 10.5 km extending about 10 km north-south. The Hartoušov mofette field is located about 10 km south from

478   the center of the main cluster, which corresponds to 6 km distance from its southern tip. A pronounced segmentation

479   of the fault plane is apparent with the 2008 and 2014 segments in the southern branch of the cluster and the 2011,

480   2017 and 2018 segments clusters in its northern branch. It is worth noting that the 2014 mainshocks showed

481   unfavorable oriented focal mechanisms and occurred on a fault jog activated by stress concentration resulting from

482   previous swarm activity (Hainzl et al., 2016, Jakoubková et al. 2018). This structural and possibly impermeable

483   boundary within the fault zone was broken by the M_L 3.5 mainshock of the 2014 sequence - the first earthquake of

484   this sequence which was followed by the massive CO_2 flow rise in Hartoušov.

485   Recently, since the summer of 2019, the CO_2 flow rate in Hartoušov F1 has decreased below 10 L/min, which could

486   be a sign of the approaching occurrence of a new seismic swarm, according to the Sibson's fault valve model.

487   However, one should also take into account that the flow rate decrease in 2019 could have been caused by the drought

488   period in the summer. The reduced groundwater pressure in the whole area would lead to the rise of the diffuse

489   component of gas flow reducing the gas discharge in the borehole. Comparing the records of groundwater level in

490   nearby mofettes with the gas flow rate in the F1 borehole however gives unequivocal results. While some correlation

491   between gas flow and water level was found for 2018 and 2019, the gas flow rate in 2017 was found independent of

492   the water level in mofettes.

493   The clear coseismic CO_2 flow rate increase during the 2008 and 2014 seismic sequences indicates the presence of a

494   *permeable channel between the southern cluster and the Hartoušov mofette field* (Fig. 9). The absence of CO_2 flow

495   anomalies coinciding with the seismic activity in northern clusters could be interpreted to show that the hydraulic

496   connection between these fault patches and the Hartoušov mofette is missing, which could be related to the afore-

497   mentioned fault jog. Besides, it is also of interest that epicenter distribution and CO_2 degassing occurrence is typically

498   separated in the area (Weinlich et al., 2006; Babuška and Plomerová, 2008); most earthquakes occur in the northern,

499   CO_2-free part of the Cheb Basin.

500   *Other monitored sites* such as Bublák and Soos show, similar to Hartoušov, almost constant CO_2 discharge since early

501   2017. As these stations were not in operation during the 2008 and 2014 seismic sequences showing coseismic CO_2

502   increase in Hartoušov, no inferences about their correlation to the seismic activity can be drawn. Bubble fractions

503   derived from resistivity measurements of the water-bubble system are found quite stable. For the measurement period

504   of four years no maintenance of the probe was required and, compared to the pressure difference method, the system

505   is less sensitive to the depth of the probe below the water table. However, no seismogenic anomaly of as flow rate has

506   occurred yet that could be used to calibrate the system. Continuous monitoring of CO_2 degassing is required to

507   determine whether future seismic activity in the southern cluster will generate an increase in degassing in either of the

508   monitored sites and enable the verification of the hypothesis that only earthquakes in the southern cluster are capable

509   of generating a CO_2 pulse which reaches the surface.

510   **5. Conclusions**

511   The present study is focused on the long-term monitoring of CO_2 degassing in the form of mofettes and gaseous

512   mineral springs targeted on the West Bohemia/Vogtland region in Central Europe, which is typified by the occurrence

513   of earthquake swarms and discharge of carbon dioxide of magmatic origin. The gas flow measurement is applied to

514   two types of sources: natural wet mofettes with gas outflow through surface water pools and boreholes tapping shallow

515   CO_2-saturated aquifers. The different local conditions of the five monitored sites call for different methods of gas

516   capture and flow rate measurement. Besides the direct flow measurement using a drum chamber gas flowmeter,

517   electronic MEMS flowmeters and Venturi-based probes we introduce a novel, indirect method based on quantifying

518   the gas bubble contents in a water column, which is capable of functioning in severe environmental conditions. The

519   method is based on measuring the pressure difference along a fixed depth interval in a water column, which is

520   proportional to the mean bubble fraction within the measured section. We analyze the dependence of the bubble

521   fraction on depth and project it to the atmospheric pressure to make it directly comparable to the gas flow rate.

522   Laboratory tests indicate the nonlinear dependence of the bubble fraction on the flow rate, which is confirmed by

523   empirical models found in the chemical and nuclear engineering literature. Flow rates and bubble fractions observed

524   in a pilot borehole F1 in the Hartoušov mofette show a high mutual correlation, however some discrepancy is found

525   between the measured flow rate and that predicted by the empirical models. This discrepancy calls for further

526   analysis.

527   We also analyzed the long-term monitoring of gas flow and bubble fraction in the pilot borehole for the period 2008

528   – 2019. We found a quite strong barometric influence on the hydraulic head of the confined aquifer corresponding to

529   a barometric efficiency of 0.76, which can be attributed to the compressibility of the pore fluids including the gaseous

530   phase of carbon dioxide.

531   The record of gas flow rate and bubble fraction in Hartoušov F1 shows two high-amplitude coseismic rises coinciding

532   with the occurrence of earthquake swarms in 2008 and 2014. The flow rate increased to a multitude of the preseismic

533   level for several months and was followed by a long-term decay. However, another three seismic swarms occurring

534   in the same fault zone were not associated with any significant CO_2 flow anomaly. We surmise that this may be related

535   to the slightly farther location of hypocenters of these swarms in comparison with the two which caused the coseismic

536   CO_2 flow rise. Further long-term CO2-flow monitoring is required to verify the mutual influence of CO_2 degassing

537   and seismic activity in the area.

Code/Data availability

Most of the data analyzed in the manuscript including email address for requesting additional data are available online at web.natur.cuni.cz/uhigug/carbonnet/en_index.html .

Author's contribution

VB and TF designed and carried out the measurements and ML formulated the theoretical part with support of TF. TF prepared the manuscript with contributions from all co-authors.

Competing interests

The authors declare that they have no conflict of interest.

Acknowledgments

CO2 flow monitoring and the work of the authors was supported by the project CzechGeo/EPOS-Sci (CZ.02.1.01/0.0/0.0/16_013/0001800). The authors thank also to Jan Vilhelm for valuable ideas.

References

Acworth R.I. and Brain T., Calculation of barometric efficiency in shallow piezometers using water levels, atmospheric and earth tide data. Hydrogeology Journal 16, 1469–1481, 2008.

Babuška V., Plomerová J., Control of paths of quaternary volcanic products in Western Bohemian Massif by rejuvenated variscan triple junction of ancient microplates. Stud. Geophys. Geod., 52, 607-629, 2008.

Babuška, V., et al., Origin of earthquake swarms in the western Bohemian Massif: Is the mantle CO_2 degassing, followed by the Cheb Basin subsidence, an essential driving force?, Tectonophysics 668-669, 42-51, http://dx.doi.org/10.1016/j.tecto.2015.12.008, 2016.

Bachura, M. and Fischer T., Detailed velocity ratio mapping during the aftershock sequence as a tool to monitor the fluid activity within the fault plane. Earth and Planetary Science Letters 453, 215–222. https://doi.org/10.1016/j.epsl.2016.08.017, 2016.

Bankwitz, P., Schneider, G., Kämpf, H., Bankwitz, E., Structural characteristics of epicentral areas in Central Europe: study case Cheb Basin (Czech Republic). J. Geodyn. 35, 5–32, 2003.

Baubron, J. C., Allard P., Toutain J. P., Diffuse volcanic emissions of carbon dioxide from Vulcano island, Italy, Nature, 344, 51–53, 1990.

Bräuer, K., Kämpf, H., Strauch, G., Weise, S.M., Isotopic evidence (^{3}He/^{4}He, ^{13}C CO_2) of fluid-triggered intraplate seismicity. J. Geophys. Res. 108 (B2), 2070. http://dx.doi.org/10.1029/2002JB002077, 2003.

Bräuer, K., Kämpf, H., Niedermann, S., Strauch, G., Tesař, J., Natural laboratory NW Bohemia: comprehensive fluid studies between 1992 and 2005 used to trace geodynamic processes. Geochem. Geophys. Geosyst. 9. http://dx.doi.org/10.1029/ 2007GC001921 (Q04018), 2008.

Bussert R., Kämpf H., Flechsig C., Hesse K., Nickschick T., Liu Q., Umlauft J., Vylita T., Wagner D., Wonik T., Flores H.E., and Alawi M., Drilling into an active mofette: pilot-hole study of the impact of CO_2-rich mantle-derived fluids on the geo–bio interaction in the western Eger Rift (Czech Republic). Sci. Dril., 23, 13–27, https://doi.org/10.5194/sd-23-13-2017, 2017.

Camarda, M., S. Gurrieri, and M. Valenza., CO_2 flux measurements in volcanic areas using the dynamic concentration method: Influence of soil permeability, J. Geophys. Res., 111, B05202, doi:10.1029/2005JB003898, 2006.

Dahm, T., Fischer, T., Velocity ratio variations in the source region of earthquake swarms obtained from arrival time double-differences. Geophys. J. Int. 196, pp. 957-970. URL: http://dx.doi.org/10.1093/gji/ggt410, 2014.

Dmytriw, A. M., Kilian, W. T., Speldrich, J. W., Beck, S. E., Morales, G., and Gehman, R. W., U.S. Patent No. 7,278,309. Washington, DC: U.S. Patent and Trademark Office, 2007.

584   Faber, E., Horálek, J., Boušková, A., Teschner, M., Koch, U., and Poggenburg, J., Continuous gas monitoring in
585   the West Bohemian earthquake area, Czech Republic: First results. Studia Geophysica et Geodaetica, 53(3), 315-328,
586   2009.

587   Fischer, T., Horálek, J., Slip-generated patterns of swarm microearthquakes from West Bohemia/Vogtland (central
588   Europe): evidence of their triggering mechanism. J. Geophys. Res. 110, B05S21.
589   http://dx.doi.org/10.1029/2004JB003363, 2005.

590   Fischer, T., Horálek, J., Hrubcová, P., Vavryčuk, V., Bräuer, K., Kämpf, H., Intra-continental earthquake swarms in
591   West-Bohemia and Vogtland: a review, Tectonophysics 611, 1-27, doi: 10.1016/j.tecto.2013.11.001, 2014.

592   Fischer, T., Matyska, C., and Heinicke., Earthquake-enhanced permeability–evidence from carbon dioxide release
593   following the ML 3.5 earthquake in West Bohemia. Earth and Planetary Science Letters, 460, 60-67, 2017.

594   Franke, W., The mid-European segment of the Variscides: tectonostratigraphic units, terrane boundaries and plate
595   tectonic evolution. In: Franke, W., Haak, V., Oncken, O., Tanner, D. (Eds.), Orogenic Processes: Quantification and
596   Modelling in the Variscan Belt, vol. 179. Geol. Soc., Spec. Publ., London, pp. 35–61, 2000.

597   Geissler, W.H., Kämpf, H., Kind, R., Klinge, K., Plenefisch, T., Horálek, J., Zedník, J., Nehybka, V., Seismic structure
598   and location of a CO_2 source in the upper mantle of the western Eger rift, Central Europe. Tectonics 24 (TC5001.
599   http://dx.doi.org/10. 10292004TC001672), 2005.

600   Ghiaasiaan, M.S., Two-phase flow, boiling and condensation in conventional and miniature systems. Cambridge
601   University Press. 636p, 2008.

602   Gurrieri, S., Valenza M., Gas transport in natural porous medium: a method for measuring soil CO_2 flows from the
603   ground in volcanic and geothermal areas, Rend. Soc. Ital. Mineral. Petrol., 43, 1151–1158, 1988.

604   Hainzl, S., Fischer, T., Indications for a successively triggered rupture growth under – lying the 2000 earthquake
605   swarm in Vogtland/NW-Bohemia. J. Geophys. Res. 107 (B12), 2338. http://dx.doi.org/10.1029/2002JB001865,
606   2002.

607   Hainzl, S., Fischer, T., Čermáková, H., Bachura, M., Vlček, J., Aftershocks triggered by fluid-intrusion: evidence for
608   the aftershock sequence occurred 2014 in West Bohemia/Vogtland. J. Geophys. Res., Solid Earth 121.
609   http://dx.doi.org/ 10.1002/2015JB012582, 2016

610   Heinicke, J., Koch, U., Slug flow — a possible explanation for hydrogeochemical earthquake precursors at Bad
611   Brambach, Germany. Pure Appl. Geophys. 157 (10), 1621–1641, 2000.

612   Horálek, J., Šílený, J., Fischer, T., Moment tensors of the January 1997 earthquake swarm in NW Bohemia (Czech
613   Republic): double-couple vs. non-double-couple events. Tectonophysics 356, 65–85, 2002.

614   Hron J., and Škuthan B., Continuing research into the pressure field of carbon-dioxide in the West-Bohemian spa
615   region (in Czech). Czech Ministry of Environment, Prague, 112 p, 2006.

616 Hrubcová, P., Geissler, W.H., Bräuer, K., Vavryčuk, V., Tomek, Č., Kämpf, H., Active magmatic underplating in
617 western Eger Rift, Central Europe. Tectonics 36. https://doi.org/10.1002/2017TC004710, 2017.

618 Jacob C.E., Fluctuations in artesian pressure produced by passing railroad-trains as shown in a well on Long Island,
619 New York. Eos Trans. AGU, 20(4), 666– 674, doi:10.1029/TR020i004p00666, 1939.

620 Jakoubková, H., Horálek, J., and Fischer, T., 2014 mainshock-aftershock activity versus earthquake swarms in West
621 Bohemia, Czech Republic. Pure and Applied Geophysics, 175(1), 109–131. https://doi.org/10.1007/s00024-017-
622 1679-7, 2018.

623 Kämpf, H., Geissler, W.H., Bräuer, K., Combined gas-geochemical and receiver func- tion studies, of the
624 Vogtland/NW-Bohemia intraplate mantle degassing field Central Europe. In: Ritter, J.R.R., Christiansen, U.R. (Eds.),
625 Mantle Plumes — A Multidisciplinary Approach. Springer-Verlag, Berlin-Heidelberg-New York, pp. 127–158., 2007.

626 Koch, U., Heinicke, J., and Voßberg, M., Hydrogeological effects of the latest Vogtland-NW Bohemian swarmquake
627 period (August to December 2000). Journal of Geodynamics, 35(1), 107-123, 2003.

628 Montoya, G.; Lucas, D.; Baglietto, E.; Liao, Y., A review on mechanisms and models for the churn-turbulent flow
629 regime. Chem. Eng. Sci. 141, 86-103. DOI 10.1016/j.ces.2015.09.011, 2016.

630 Nickschick T., Kämpf H., Flechsig C., Mrlina J., Heinicke J., CO_2 degassing in the Hartoušov mofette area, western
631 Eger Rift, imaged by CO_2 mapping and geoelectrical and gravity surveys. Int J Earth Sci., 2015.

632 Roeloffs, E., Poroelastic techniques in the study of earthquake=related hydrologic phenomena, Advances in
633 Geophysics, 37, 135-195, 1996.

634 Rojstaczer, S. and Riley F. S., Response of the water level in a well to Earth tides and atmospheric loading under
635 unconfined conditions. Water Resources Research, 26 (8), 1803-1817, 1990.

636 Sander, R., Compilation of Henry's law constants (version 4.0) for water as solvent. Atmos. Chem. Phys., 15, 4399-
637 4981, DOI 10.5194/acp-15-4399-2015, 2015.

638 Sibson, R.H., Implications of fault-valve behavior for rupture nucleation and recurrence. Tectonophysics 211, 283–
639 293, 1992.

640 Škuthan B., Hron J., Pěček J. and Keprta M., Carbon dioxide field in the West Bohemian Spring Region: Introductory
641 results. Bull. Czech Geol. Surv., 76/4, 203−208, 2001.

642 Špičák, A., Horálek, J., Migration of events during the January 1997 earthquake swarm (The West Bohemia–Vogtland
643 region). Stud. Geophys. Geod. 44, 227–232, 2000.

644 Špičáková, L., Uličný, D., Koudelková, G., Tectonosedimentary evolution of the Cheb Basin (NW Bohemia, Czech
645 Republic) between Late Oligocene and Pliocene: a preliminary note. Studia Geophys. Geod. 44, 556–580, 2000.

646 Todd D.K., 1980. Groundwater Hydrology. 2d ed. New York: John Wiley & Sons.

647 Vavryčuk, V., Non-double-couple earthquakes of January 1997 in West Bohemia, Czech Republic: evidence of tensile

648 faulting. Geophys. J. Int. 149, 364–373. http://dx.doi.org/10.1046/j.1365-246X.2002.01654.x, 2002.

649 Vavryčuk, V., Principal earthquakes: theory and observations from the 2008 West Bohemia swarm. Earth Planet. Sci.

650 Lett. 305, 290–296. http://dx.doi.org/10.1016/ j.epsl.2011.03.002, 2011.

651 Vavryčuk, V., and P. Hrubcová, Seismological evidence of fault weakening due to erosion by fluids from observations

652 of intraplate earthquake swarms, J. Geophys. Res. Solid Earth, 122, doi:10.1002/2017JB013958, 2017.

653 Weinlich, F.H., Bräuer, K., Kämpf, H., Strauch, G., Tesar, J., Weise, S.M., An active sub – continental mantle volatile

654 system in the western Eger rift, Central Europe: gas flux, isotopic (He, C, and N) and compositional fingerprints.

655 Geochim. Cosmochim. Acta 63, 3653–3671. http://dx.doi.org/10.1016/S0016-7037(99)00187-8, 1999.

656 Weinlich, F. H., Faber, E., Boušková, A., Horálek, J., Teschner, M., and Poggenburg, J., Seismically induced

657 variations in Mariánské Lázně fault gas composition in the NW Bohemian swarm quake region, Czech Republic—A

658 continuous gas monitoring. Tectonophysics, 421(1), 89-110, 2006.

659 Ziegler, P.A., European Cenozoic rift system. Tectonophysics 208, 91–111, 1992.

660 Zuber, N., and Findlay, J., Average volumetric concentration in two-phase flow systems. Journal of heat transfer,

661 87(4), 453-468, 1965

662

663

664

665
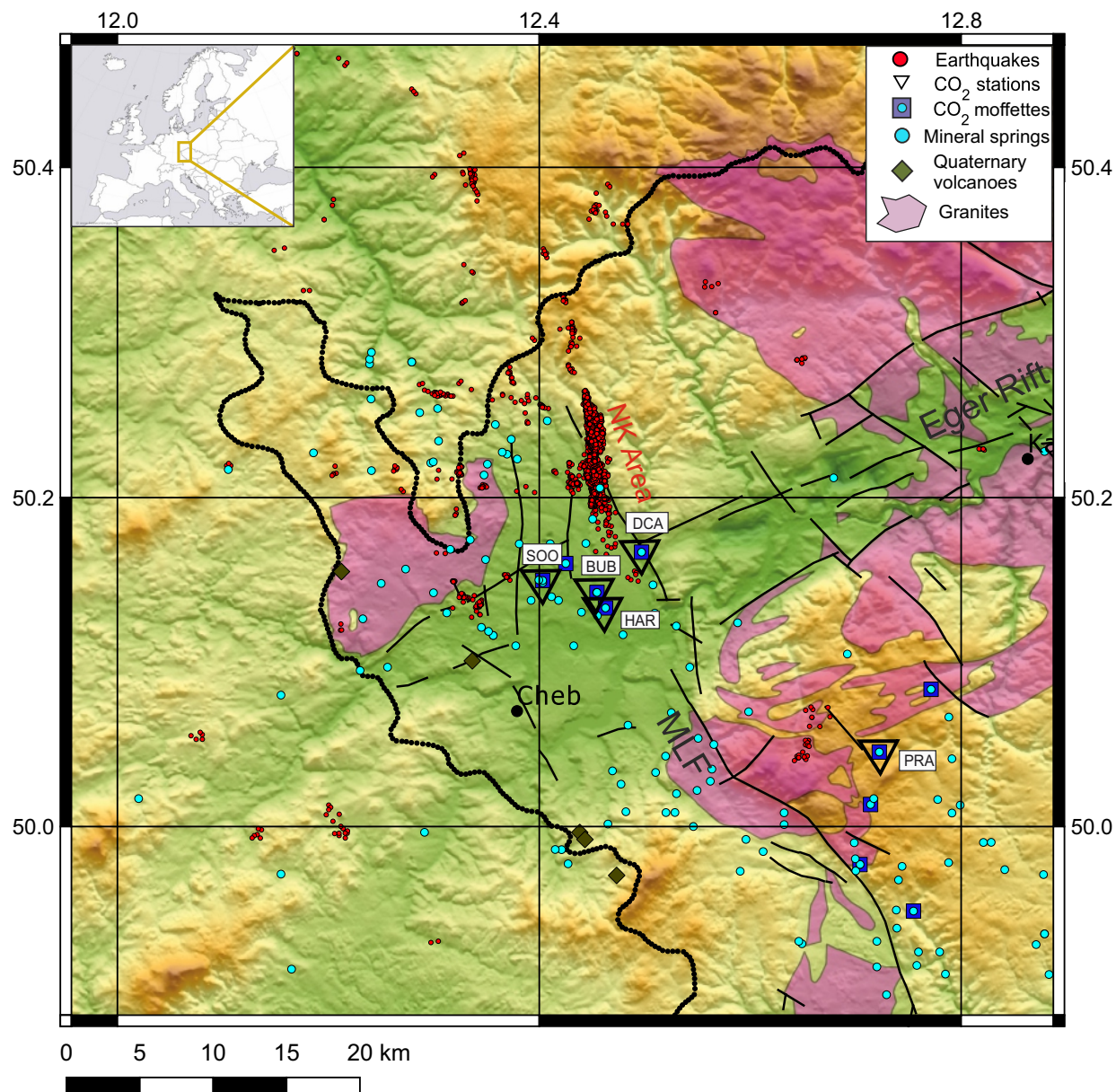
666 Figure 1. Relief map of the West Bohemia/Vogtland region with the fault network, granite units, and major fault zones as Mariánské
667 Lázně Fault (MLF) and Eger Rift. Seismic events, major focal zone of Nový Kostel (NK Area), CO_2 monitoring stations, CO_2
668 mofettes and mineral springs and Quaternary volcanoes are also indicated (see the legend).

669

670

671

672

673   Figure 2. Photos of selected CO_2 monitoring fields – Hartoušov, SOOS, Bublák and Prameny

674

675

678   a)   b)
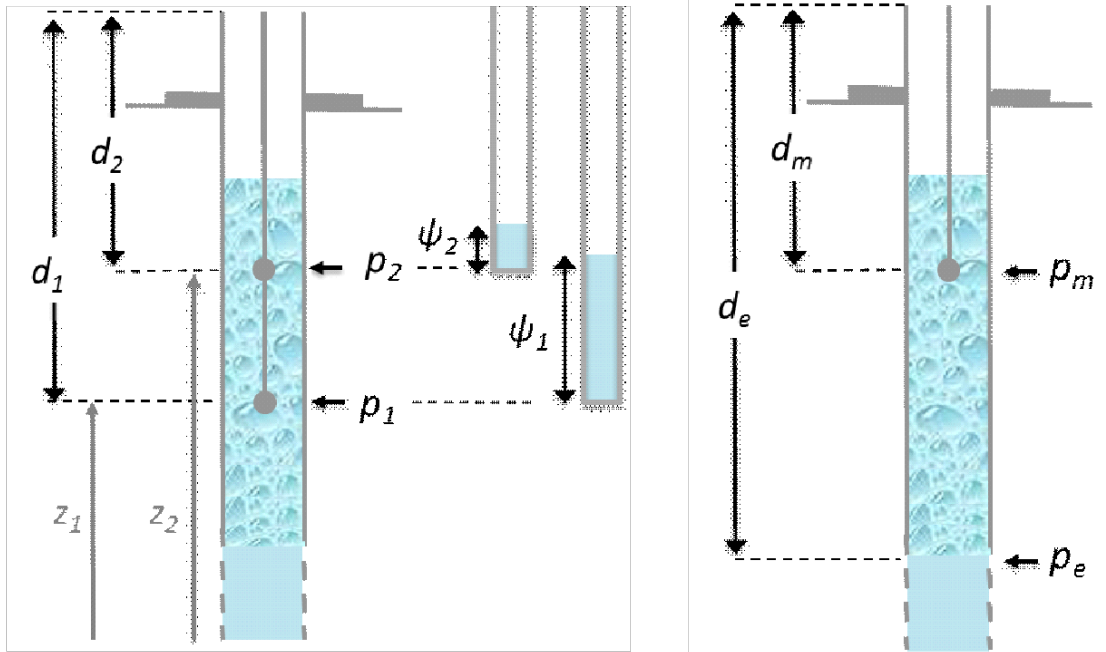
679   Figure 3. Measurement of pressure in the borehole with ascending bubbles: the measured pressure p and the related pressure head
680   ψ at two different depths d_1 and d_2 within the bubble column using the *differential method* (a); pressure within the bubble column
681   p_m and beneath p_e used to determine the mean bubble fraction using the *integral method* (b). Note that the difference of altitudes
682    $z_2 - z_1 = d_e - d_m$.

683

684

685

686

687
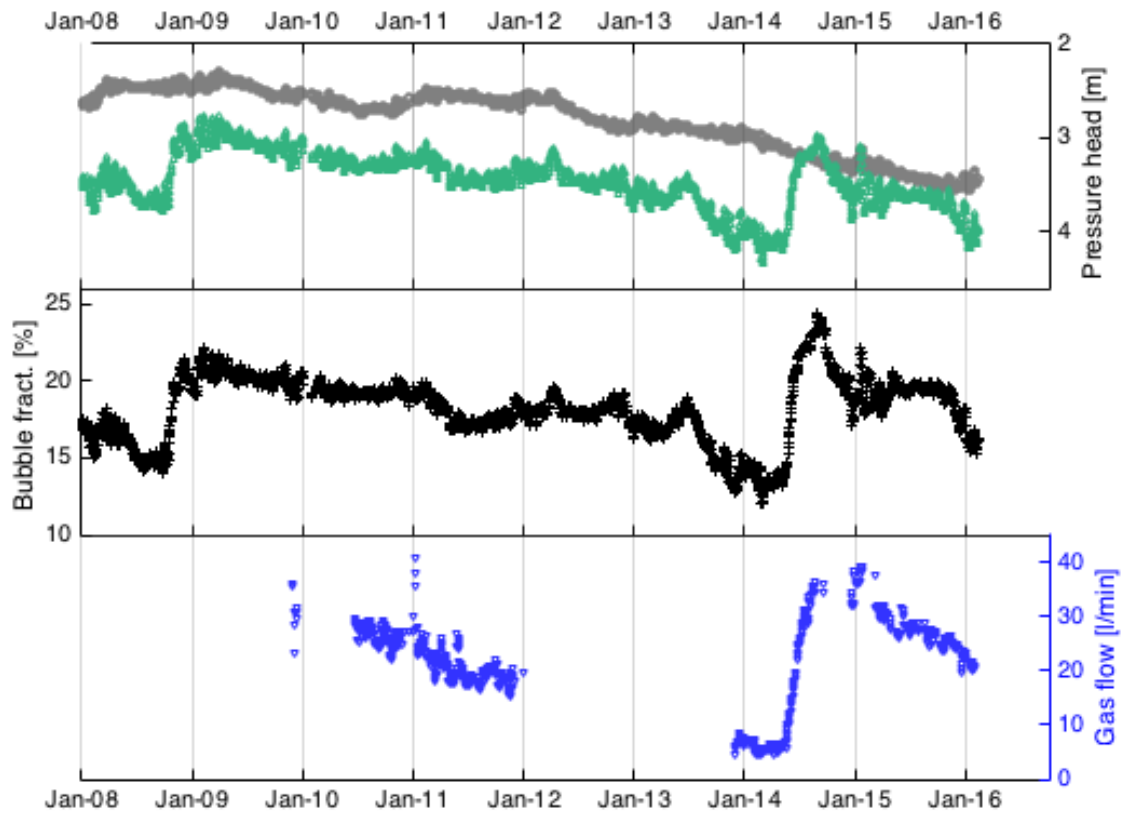
688 Figure 4. Daily averages of the reference pressure head h_e (grey) unaffected by gas flow and in the monitored Hartoušov F1 well,
689 h_m (green); the volumetric fraction of bubbles (black) determined by Eq. 4 and CO_2 flow (blue) in the Hartoušov F1 well for the
690 period 2008-2016. Because no reference pressure measurement below the bubble entry point was available for the studied period,
691 a pressure head in nearby Hrzín borehole, which was free of gas flow, was used as h_e.

692

693

694
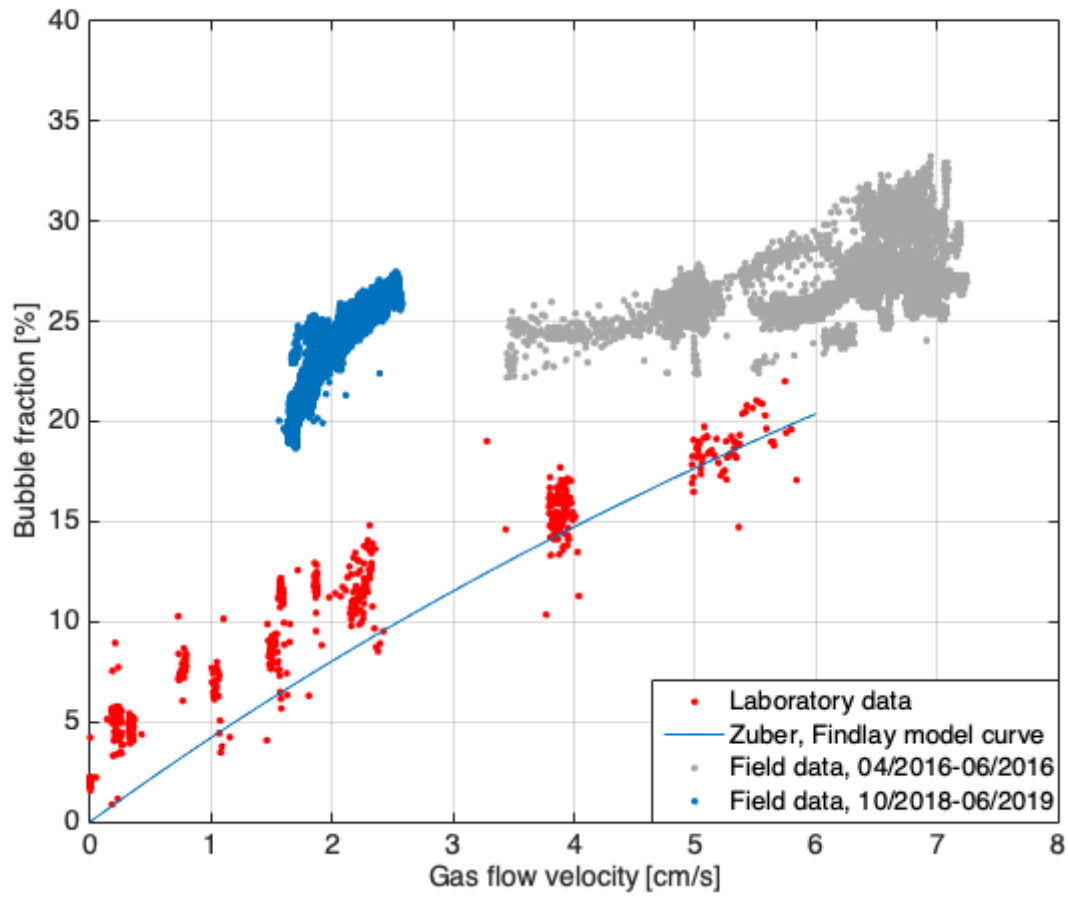
Figure 5. Comparison of gas flow velocity and volumetric fraction of bubbles for the field (Hartoušov mofette) and laboratory
measurement. Laboratory measurements are smoothed by RC circuit of 30 s time constant (red points) and additionally by running
average of 1 min length; the field measurements from 2016 (grey points) are based on the differential method with sensor distance
of 1.0 m; the field measurements from 2018-2019 (blue points) are based on the integral method. Blue line is the best fit based on
eq. (5).

700

701

702
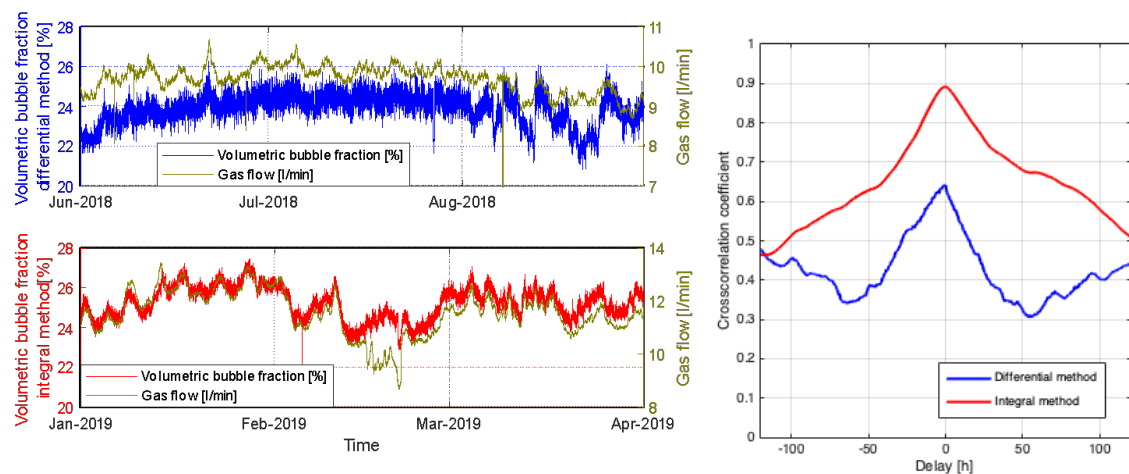
703 Figure 6. Comparison of volumetric bubble fraction derived using   differential (top left) and integral (bottom left) methods with
704 the gas flow at the Hartoušov F1 borehole. Depth of pressure probes for the differential method are 4.45 and 5.45 m below the
705 surface. For the integral method it is 5.45 m and 27.2 m. On the right the cross-correlation functions between the bubble fraction
706 and gas flow rate are shown.

707

708

709   a)   b)

710
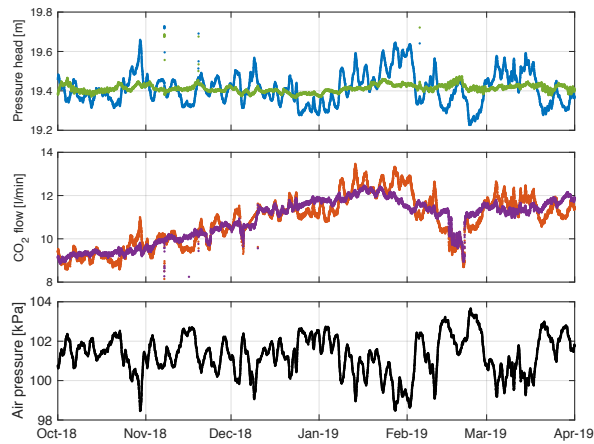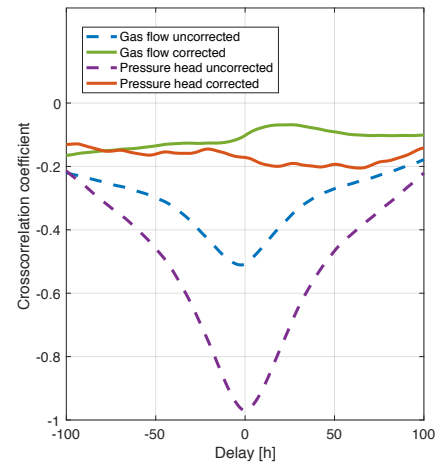
Figure 7. The barometric effect to the pressure head and CO_2 flow in the Hartoušov F1 borehole for the period from October 2018 to April 2019. a) Original measurements are indicated in blue and those corrected for barometric pressure are in red. The upper panel shows pressure head at the depth below the bubble formation and the lower panel shows gas flow measured by flowmeter. The success of barometric correction is illustrated in b) showing the decrease of barometric anticorrelation after correcting.

715

716

717   a)

718

719   b)

720
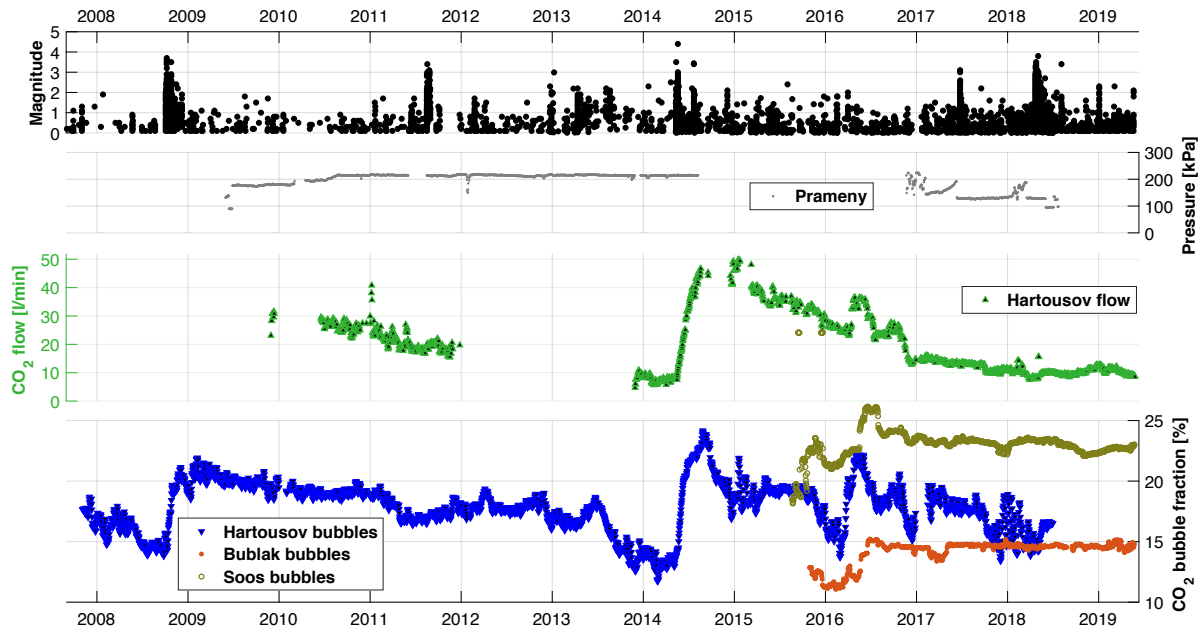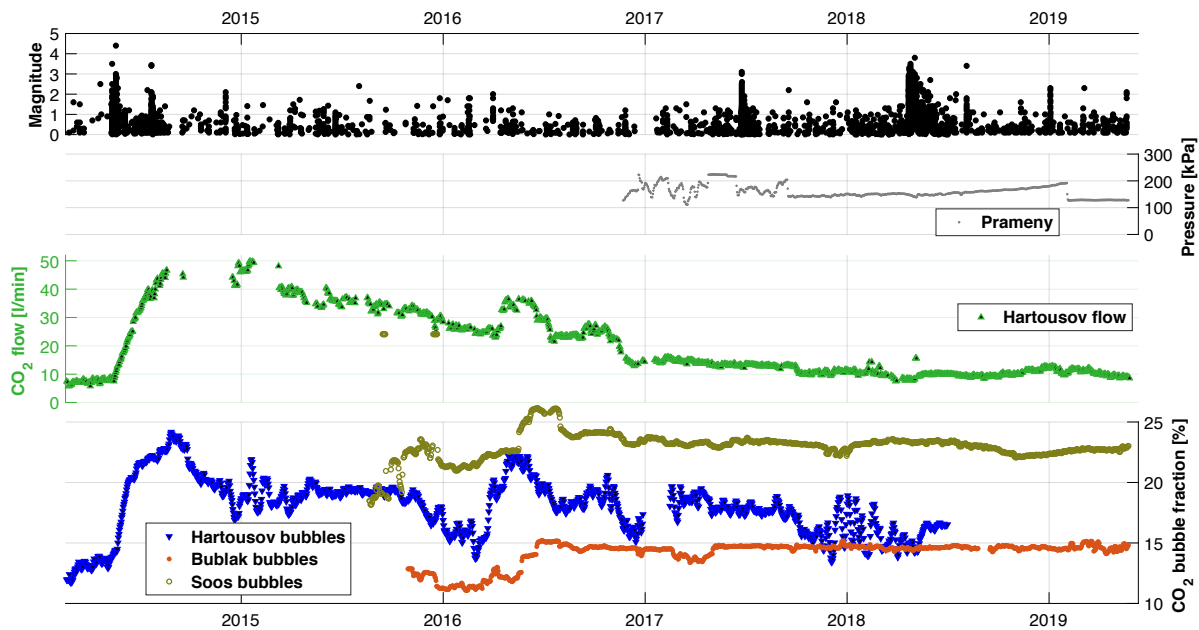
Figure 8. Comparison of seismic activity and CO_2 production at individual monitoring sites in West Bohemia. For Hartoušov F1 the CO_2 flow and gas bubble fraction are shown; for Bublák and Soos the CO_2 bubble fraction is shown and for Prameny the gas pressure in a closed borehole is plotted; (a) period 2007-2019; (b) detail for the period 2014-2019. Gas bubble fraction was determined using the pressure difference method in the integral version for Hartoušov (blue), in differential version for Bublák (red) and by the resistivity method for Soos (light brown).

726

727
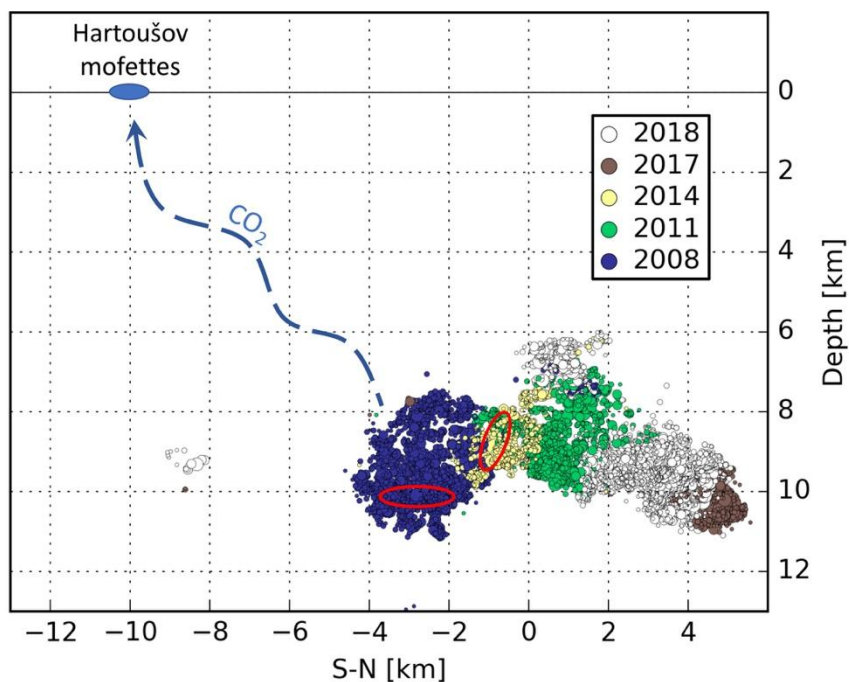
728 Figure 9. Vertical, north-south oriented section through the Nový Kostel fault zone with hypocenters of the earthquake swarms
729 occurred between 2008 and 2018. The position of the Hartoušov mofette showing coseismic CO_2 flow rate increase is indicated on
730 the surface. Red ovals show the position of first events of the 2008 and 2014 seismic sequences.